# A Theoretical Model for Quantifying Expansion of Intumescent Coating Under Different Heating Conditions

**Burak Kaan Cirpici,[1] Y.C. Wang,[2] B.D. Rogers,[2] S. Bourbigot[3]**
[1] *Corlu Engineering Faculty, Civil Engineering Department, Namik Kemal University, Turkey*
[2] *School of Mechanical, Aerospace and Civil Engineering, University of Manchester, United Kingdom*
[3] *R2Fire Group/UMET - UMR CNRS 8207, Ecole Nationale Superieure de Chimie de Lille (ENSCL), University of Lille, 59652 Villeneuve d'Ascq, France*

**This article presents an analytical method to calculate the expansion of intumescent coatings under different heating and fire conditions, being the most critical step in quantifying their fire protection performance under different conditions. The proposed method extends that of Amon and Denson, originally developed for spherical bubbles in viscous fluid subject to increase in pressure within the bubbles, to intumescent coatings with non-uniform temperature field and temperature-dependent viscosity. The pressure increase inside the bubbles is a result of the conversion of intumescent coatings from melt to gases at high temperatures. The extended analytical method has been used to predict the expansion processes of intumescent coatings tested by Zhang et al. under cone calorimeter with different heating rates and under furnace fire condition with different temperature–time curves, and those of Muller under cone calorimeter heating. In these tests, intumescent coatings were applied to steel plates and the tests examined the effects of different coating thicknesses and steel plate thicknesses, therefore allowing the fire and cone calorimeter tests to encompass a wide range of temperatures and rates of heating. Comparison of the analytical calculation and test results indicates that the proposed method is suitable for quantifying the expansion process of intumescent coatings.** **POLYM. ENG. SCI., 56:798–809, 2016.** **© 2016 Society of Plastics Engineers**

## INTRODUCTION

Intumescent coatings are widely used as fire protection material for building structures, especially steel-framed buildings, to provide them with sufficient fire resistance. For onshore applications, where the fire exposure is cellulosic, thin film intumescent coatings are the preferred choice because they are flexible and ease to use and can be employed to enhance aesthetics appearance.

Intumescent coatings are inert at room temperature but when they are exposed to heat, they undergo a series of chemical reactions which can make the intumescent coatings swell up to 100 times of the initial thickness, forming a cellular char. It is this expanded char, which has low thermal conductivity, that acts as a barrier to protect the steel substrate against fire attack. Intumescent coatings are reactive materials and the chemical reactions depend on many factors, the two most important of which are the heating temperature and the rate of heating. Because of the complexity of intumescent coating behaviour in fire, assessment of the performance of intumescent coatings is based on conducting numerous fire tests, which is not an effective process. Furthermore, the current Eurocode [1] for the assessment of intumescent coating properties is only applicable to the standard fire condition and does not reflect the effects of different substrate steel thicknesses and intumescent coating thicknesses.

Appropriate assessment of intumescent coating performance requires a thorough understanding of the fundamental characteristics of intumescent coatings. When an intumescent coating is exposed to heat, it melts into a viscous fluid. Gases are then released, from the blowing agent, to expand the viscous fluid. Afterwards, the intumescent coating solidifies to form a stable char layer. The expanding process and the final expansion are the most critical factors that determine the fire protection performance of the intumescent coating.

A number of different models have been proposed to estimate the expansion of intumescent coatings. In the previous studies of Cagliostro et al. [2], Anderson et al. [3], Henderson and Wiecek [4], the maximum expansion was assumed. With the maximum expansion being treated as input data, these research studies then proceeded to conduct heat transfer analysis by treating intumescent coatings as non-reactive material. Di Blasi and Branca [5] and Di Blasi [6] developed a much more complex set of formulations to analyse heat and mass transfer in intumescent coatings, but they again assumed the final expansions of intumescent coatings were known *a prior*. Yuan and Wang [7] adopted the approach of Di Blasi [6] and investigated the influences of different intumescent coating properties on intumescent coating thermal conductivity and protected steel temperatures. The internal structure of intumescent coating char, in particular, the average bubble size, was identified to have some influence on intumescent coating thermal conductivity. The maximum expansion ratio was found to be most influential. Butler et al. [8] attempted to model intumescent coating expansion at the microscopic level, considering heat transfer, hydrodynamics and mass transfer. Although this modelling demonstrated the potential of this approach, the modelling was limited to the very early stage of intumescent coating behaviour.

The research that is most relevant to the current work comes from that of Zhang et al. [9] and Zhang et al. [10] where they attempted to predict the expansion process of intumescent coatings. In their model, they assume that the expansion ratio of intumescent coatings is directly proportional to the ratio of density of the solid blowing agent to the released gas density, assuming that the intumescent coating pressure is maintained at the atmospheric

*Correspondence to*: Y.C. Wang; e-mail: yong.wang@manchester.ac.uk
Previous address: B.K. Cirpici; School of Mechanical, Aerospace and Civil Engineering, University of Manchester, UK.
This article was published online on 30 March 2016. A late request by the authors to add a Previous address footnote was made. This notice is included in the online and print versions to indicate that both have been corrected 18 April 2016.
DOI 10.1002/pen.24308
Published online in Wiley Online Library (wileyonlinelibrary.com).

pressure. Because this would result in final expansion ratios of hundreds of times (the ratio of density of solid intumescent coating to gas is about 1300), they stipulated that only a fraction of the released gas would be retained (trapped) in the intumescent coatings to cause expansion. They then proposed a hypothetic link between the amount of trapped gas, as a proportion of the total gas released, and the temperature and heating rate. They have compared their predictions against their own cone calorimeter Zhang et al. [10] and furnace fire Zhang et al. [9] tests. Although their comparisons show good agreement between their model prediction and test results, their assumption that most of the released gas escapes from the intumescent coating during the expansion process is highly questionable because this would require the released gas from inside the intumescent melt to travel through the coating and further to the outside air almost instantly when they are released.

The purpose of this study is to test a different hypothesis. It assumes that all of the released gases are retained in the intumescent melt. However, expansion of the released gases is subject to pressure by the surrounding viscous intumescent melt. After the expanded intumescent coating has formed a char, cracks may form in the char and the pressurised gases inside the gas bubbles may indeed release to the outside air, but the expansion that has already happened would be maintained.

To test this alternative theory of intumescent coating expansion, the mathematical (cell) model of Amon and Denson [11] will be applied. Starting from the basic principles of mass and momentum conservation, Amon and Denson [11] developed a theoretical model to calculate the expansion of spherical bubbles in viscous fluid when the pressure inside the bubbles increases. They assumed that all physical properties of the fluid and the gas were constant. However, despite these simplifying assumptions, the resulting analytical solution may still apply, provided modifications are made to take into consideration the source of pressure increase inside the intumescent coating bubbles and changes in intumescent coating properties at high temperatures, which can be done through implementing a time-increment approach.

Therefore, the aim of this article is to test feasibility of applying the Amon and Denson [11] model for predicting intumescent coating expansion. For checking accuracy of this extension, the analytical model results will be compared against the cone and furnace fire test results of Zhang et al. [9] and Zhang et al. [10], and the cone calorimeter test results of Muller [12].

## A BRIEF DESCRIPTION OF THE MATHEMATICAL MODEL OF AMON AND DENSON AND ITS APPLICATION TO INTUMESCENT COATINGS

### *A Brief Introduction to the Amon and Denson Theory*

Amon and Denson [11] have proposed a mathematic model to describe how spherical bubbles in a polymer liquid will expand when the interior pressure inside the bubbles is increased. Refer to Fig. 1, which shows uniformly distributed bubbles of radius $R$, within a viscous polymer liquid that has a viscosity $\mu$. Each bubble has an envelope of radius "$S$." On the basis of the conservation of mass and momentum, Amon and Denson [11] have obtained the following equation to describe the expansion ratio of the bubbles:

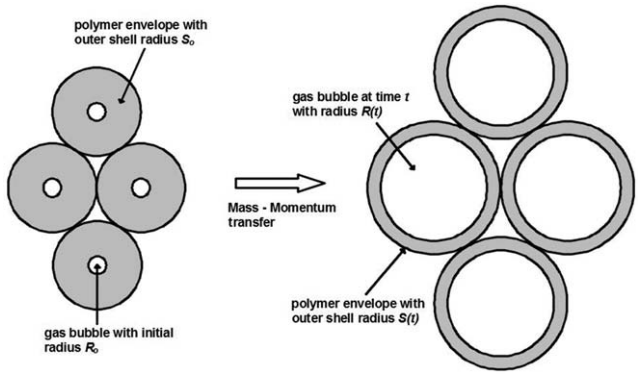


FIG. 1. Schematic representation of the multi-cell model [11].

$$\frac{dR}{dt}=R\left(\frac{P_g-P_a-2\sigma/R}{4\eta}\right)\left(\frac{S^3-R^3}{S^3}\right) \tag{1}$$

where $S(t)$ and $R(t)$ are the radius of the bubble and the outer shell respectively at time $t$, with initial values of $R_0$ and $S_0$ respectively, $\eta$ is the viscosity of the surrounding liquid and $\sigma$ is the bubble surface tension. By conservation of volume,

$$S(t)=\left({S_0}^3+R(t)^3-{R_0}^3\right)^{1/3} \tag{2}$$

The outer shell radius $S(t)$ calculated at each time step.

The initial outer shell radius is calculated by using the nucleation density, that is, the number of nucleation sites per volume, $N/V$.

$$S_0=\left[\frac{3}{4\pi N_{cells}}\right]^{1/3} \tag{3}$$

All nucleated cells are uniformly distributed and each cell has $[(4/3)\pi]{S_0}^3$ volume at $t=0$.

The initial outer shell radius, $S_0$ significantly greater than the initial bubble radius $R_0$. Figure 1 shows a schematic representation of the cell model.

In deriving the above equation, Amon and Denson [11] have made the following assumptions:

The gas inside the bubble is based on ideal gas law and there is thermodynamic equilibrium at all times at the gas–liquid interface according to gas concentration (Henry law).

The liquid in the polymer shell is incompressible and Newtonian fluid.

Material properties of the polymer fluid do not change with time.

Coalescence of the bubbles is negligible and the number of bubble per unit volume ($N_{\text{cells}}$–number of nucleated cells per unit volume) does not change throughout the expansion process

### *Application to Intumescent Coatings*

In this research, the Amon and Denson [11] bubble growth model has been applied to modelling the expansion of intumescent coatings with the following adaptations:

Expansion of the intumescent coatings is assumed to be one-dimensional, perpendicular to the direction of heating. In the

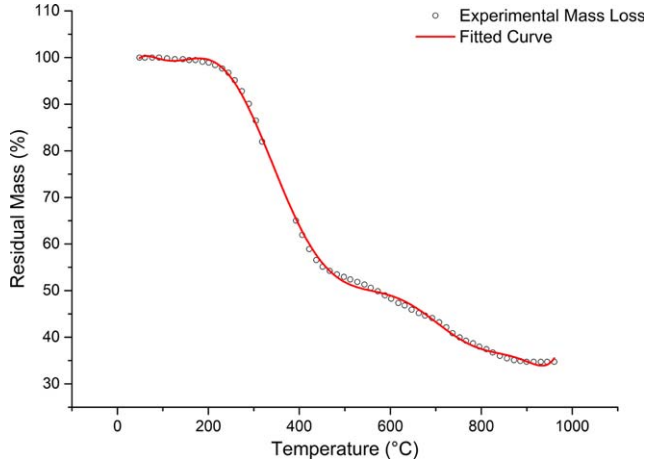


FIG. 2. Mass conversion (loss) data as a function of temperature for intumescent coatings of Zhang et al. [10]. [Color figure can be viewed in the online issue, which is available at wileyonlinelibrary.com.]

coating thickness direction, the coating is divided into a large number of layers, each of which has the same temperature.

The driving force (pressure) inside the bubbles is due to the release of additional gases from the intumescent coating melt. All the released gases are trapped inside the coating and there is no diffusion of the released gases.

Thermodynamic equilibrium is instantly achieved with changing temperatures.

The material properties of the intumescent coating (viscosity, gas release, surface tension) change with temperature and time (Section "*Input Properties of Intumescent Coating*").

*Input Properties of Intumescent Coating*

The analytical model of Amon and Denson [11] is used to model the tests of Zhang et al. on intumescent coatings under the cone calorimeter heating condition [10] and furnace fire [9], and the cone calorimeter tests of Muller [12].

**Mass Conversion (Loss).** In the literature on intumescent coatings, the conversion of intumescent melt into gases is often referred to as mass loss. This is a misconception because the intumescent melt mass that has been converted into gases have not been lost. However, this is understandable because such tests are carried out using very small volumes and small quantities of intumescent coating mass in thermogravimetric analysis (TGA) tests. Because of the small sample size in the TGA test, the released gases can easily escape, hence giving rise to the appearance of mass loss. However, in large test samples such as in cone calorimeter or furnace fire tests that are modelled in this study, the gases are assumed to be retained. Thus, the mass loss from the TGA test is alternatively referred to mass conversion in this paper.

Figure 2 shows the mass conversion–temperature relationships for the intumescent coatings studied by Zhang et al. [10] and Fig. 3 provides the same data for the intumescent coatings studied by Muller [12]. The fitted curves will be used in the predictive model of this article. The intumescent coatings used by Zhang et al. [9, 10] were water based and those by Muller [12] were solvent based.

**Pressure Increase.** The mass conversion value can be used to calculate the pressure increases inside intumescent coating bubbles that drive the expansion process. Consider an initial bubble of volume $V$. When the intumescent coating is converted from melt to gases, assume the mass of the total converted gas is $\Delta m$ sociated with the bubble volume $V$. If the pressure inside the bubble is maintained, the bubble would have to increase in volume by:

$$\Delta V = \Delta m/\rho_g \tag{4}$$

where $\rho_g$ is the density of the gases inside the bubble.

However, before expansion occurs, the volume of the bubble is maintained. Therefore, the pressure inside the bubble has to increase. According to the ideal gas law, the initial state of the bubble is:

$$P_a V = nRT \tag{5}$$

where $R$ is the ideal gas constant, $n$ is the amount of gas in mole, $V$ is the volume of the gas and $T$ is temperature. $n = \frac{m}{MW}$ in which $M$ is the mass of gas and $MW$ is the molar mass.

With the volume unchanged and the temperature maintained, when the additional $\Delta m$ is included, the state of the bubble is:

$$(P+\Delta P)V = (n+\Delta n)RT \tag{6}$$

where $\Delta n = \frac{\Delta m}{MW}$.

Therefore, the new pressure in the bubble can be calculated using:

$$\frac{P_g}{P_a} = \frac{(m+\Delta m)}{m} = \frac{(V+\Delta V)}{V} \tag{7}$$

$$P_g = \frac{\Delta V + V}{V} P_a \tag{8}$$

where $P_a$ the initial gas pressure inside the bubble before mass conversion and expansion.

**Surface Tension.** To use *Eq. 1*, the surface tension of the intumescent coating melt is required. Since there has been no

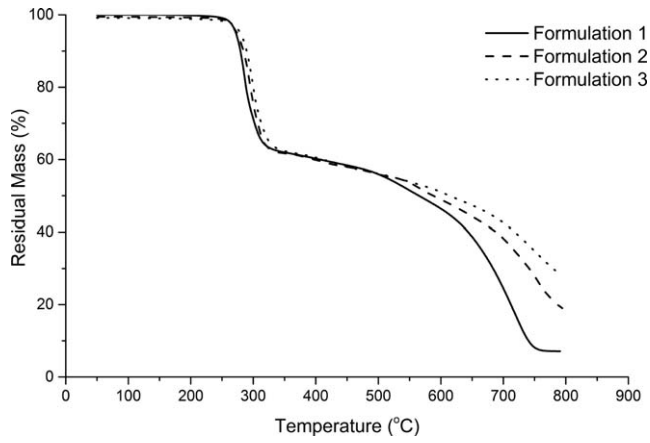


FIG. 3. Mass conversion (loss) data as a function of temperature for intumescent coatings of Muller [12].


DOI 10.1002/pen

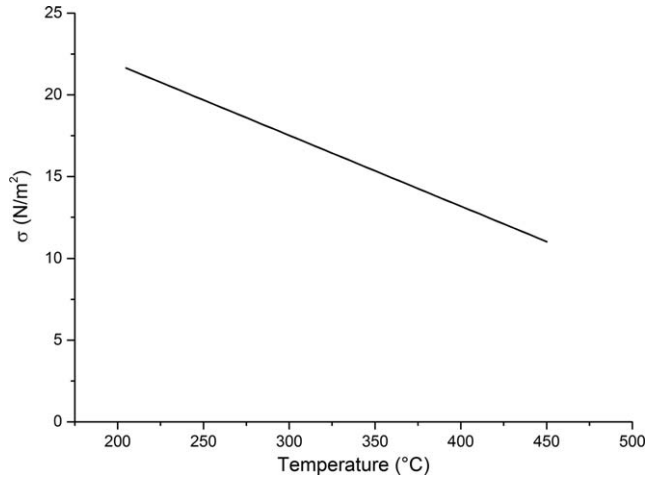


FIG. 4. Surface tension versus temperature for polyethylene melt [13].

measurement of this property for intumescent coating melt, the values of Kwok et al. [13] for polyethylene are adopted. This is shown in Fig. 4.

Fortunately, prediction of intumescent coating expansion is not sensitive to the value of surface tension. For example, Fig. 5 indicates that when using the variable surface tension in Fig. 4 and a constant value of 20 N/m$^2$ for predicting one (C12L1) of the tests of Zhang et al. [10], the results nearly coincide.

**Viscosity.** For the intumescent coating studied by Zhang et al. [9, 10], there was no measurement of viscosity. Therefore, for the purpose of this aricle, the viscosity value has to be estimated. This estimate is based on the results of Bugajny et al. [14] which provided viscosity data for a number of intumescent melts given by Bourbigot et al. [15]. These data are shown in Figs. 6 and 7. Comparing the mass conversion (loss) data shown in Fig. 2 for the intumescent coatings studied by Zhang et al. [10] with the TGA data of Fig. 6, it can be seen that of the intumescent coatings of Zhang et al. [10] is similar to the curve for PP-APP/PER. Therefore, in this article, it is assumed that the viscosity of the intumescent coatings studied by Zhang et al. [10] is that of curve for PP-APP/PER. Figure 7 shows the

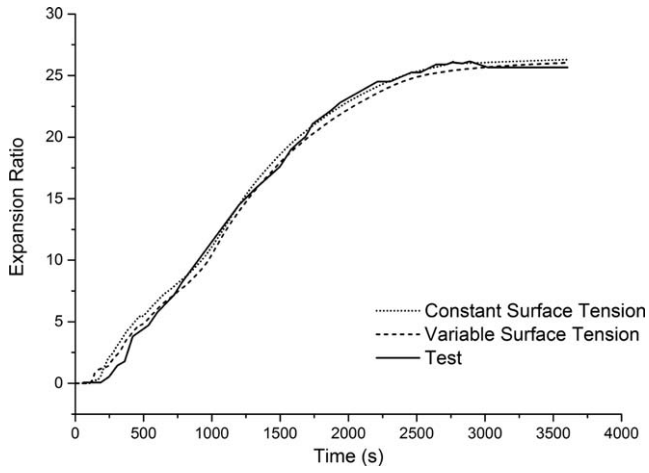


FIG. 5. Sensitivity of intumescent coating expansion ratios to surface tension.

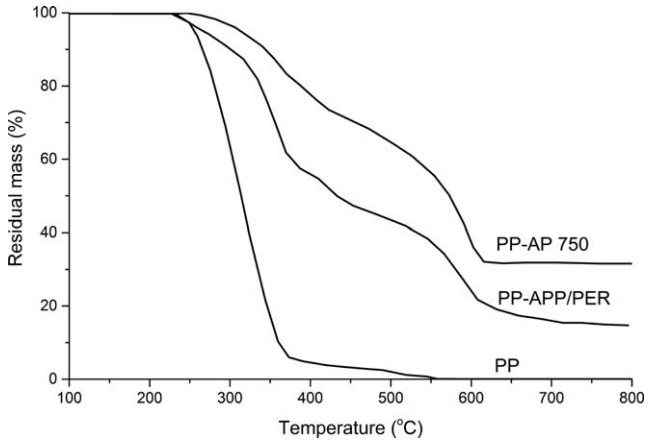


FIG. 6. TGA curves of different mixture of intumescent coatings [15].

recorded viscosity–temperature relationship for PP-APP/PER and the fitted polynomial curve for use in this article. Figure 8 shows the measured viscosity–temperature relationships for the intumescent coatings of Muller [12].

## MATHEMATICAL MODEL RESULTS AND COMPARISON

Zhang et al. [9, 10] carried out two series of tests, one under furnace fire exposure and one under cone calorimeter. Muller [12] performed cone calorimeter tests using different intumescent coating formulations. Comparison will be made for these three series of tests.

### *Comparison for Furnace Fire Tests*

The furnace fire tests of Zhang et al. [9] were conducted by placing intumescent coated steel plates, all measuring 100 mm by 100 mm in planar dimensions but different plates having different thicknesses, each with the same intumescent coating thickness on both sides, to fire exposure from both sides. Three fire temperature-time curves were used for the furnace fire test condition. They are shown in Fig. 9 and are referred to as Fast fire, ISO fire and Slow fire.

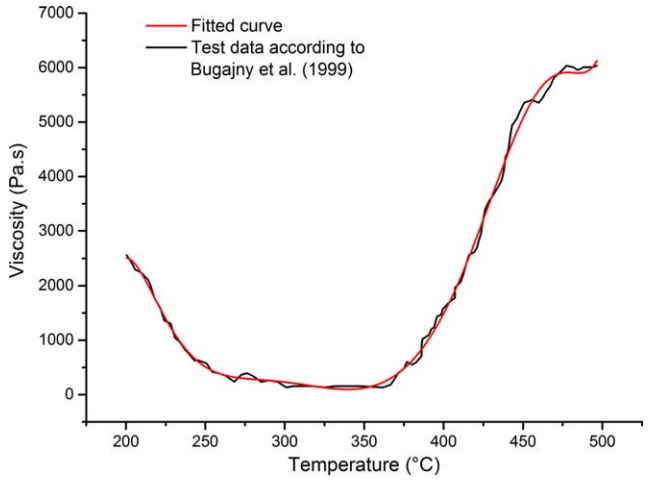


FIG. 7. Assumed viscosity–temperature relationship, based on heat-treated PP/PER/APP system of Bugajny et al. [14]. [Color figure can be viewed in the online issue, which is available at wileyonlinelibrary.com.]

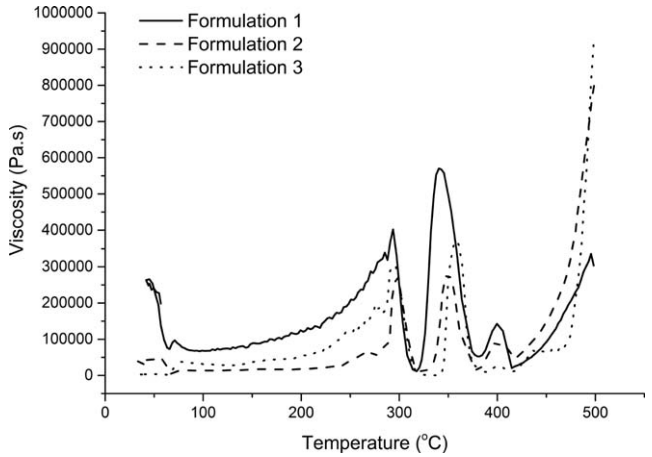


FIG. 8. Viscosity–temperature relationships for the intumescent coatings of Muller [12].

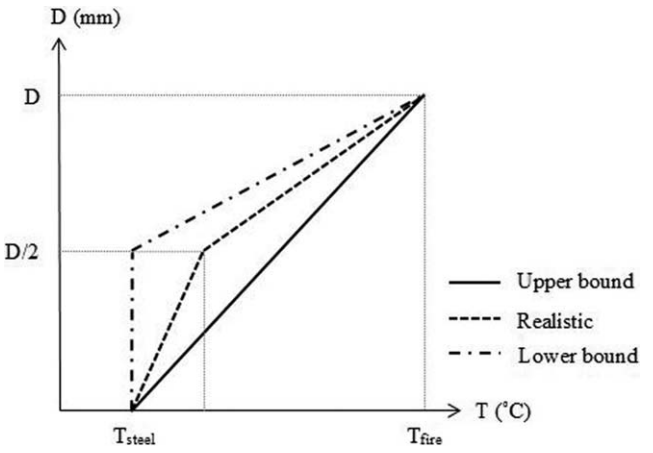


FIG. 10. Different possible temperature assumptions throughout the intumescent coating thickness (D: Coating thickness, T: Temperature).

When the intumescent coating protected steel plate was exposed to fire, the temperature distribution in the intumescent coating was non-uniform. When using the Amon and Denson model, the intumescent coating was divided into a large number of slices, each of the slices having its own uniform temperature. The temperatures of these slices are based on the assumed temperature distributions shown in Fig. 10. In this figure, the temperature of the intumescent coating in contact with the fire has the same temperature as the fire and that in contact with the steel plate the same temperature as the steel plate.

Because of the very small mass of intumescent coatings used, the effect of heat capacitance in heat transfer may be neglected. Therefore, heat transfer within the intumescent coating may be considered steady state. Under this condition, the temperature gradient within the intumescent coating is inversely proportional to the thermal conductivity of intumescent coating. The effective thermal conductivity (based on the original thickness) of intumescent coatings decreases as the temperature increases. Therefore, it is expected that the temperature gradient within the intumescent coating increases from the steel plate side to the fire side. The two temperature distribution bounds in Fig. 10 represent the possible lower and upper bounds with the middle distribution in Fig. 10 representing possible realistic temperature distribution inside the intumescent coating. The three temperature distributions in Fig. 10 are used to demonstrate sensitivity of the calculating results using the Amon and Denson model to the assumed temperature distribution.

The steel plate thicknesses were 5, 10, and 20 mm/s and the nominal dry film thicknesses (DFTs) were 0.4, 0.8, and 1.2 mm, respectively. However, in this modelling, the actual measured DFTs were used.

In the following sections, A, B, and C refer to 5, 10, and 20 mm steel plate thicknesses, respectively, whereas 04, 08, 12 refer to 0.4, 0.8, and 1.2 mm DFTs, respectively. For example, A04SLOW refers to a 6 mm thick steel plate with 0.4 mm DFT subjected to slow fire condition.

## RESULTS AND DISCUSSION

*Sensitivity of Modelling Results to the Number of Nucleation Sites*

When intumescent coating starts to expand, many bubbles will be created at different nucleation sites. The Amon and Denson model calculates expansion of the bubbles, from which the total expansion of the intumescent coating is calculated, as

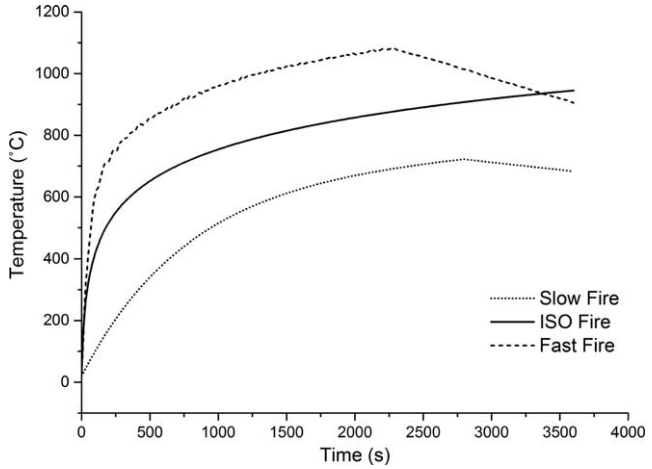


FIG. 9. Furnace fire–temperature curves [9].

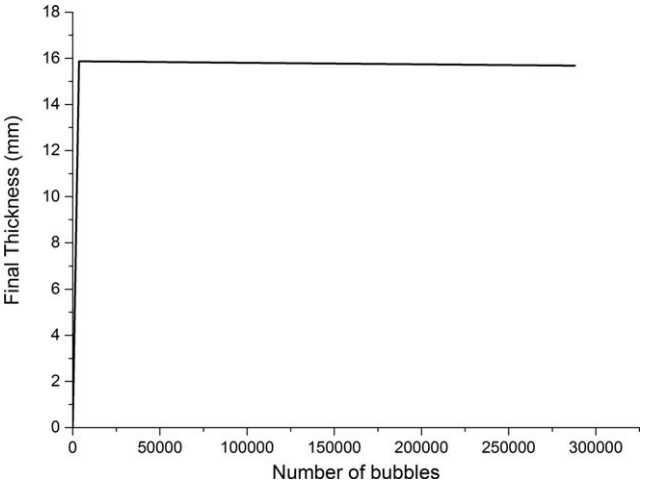


FIG. 11. Effect of number of bubbles on the final expanded thickness of intumescent coating.


DOI 10.1002/pen

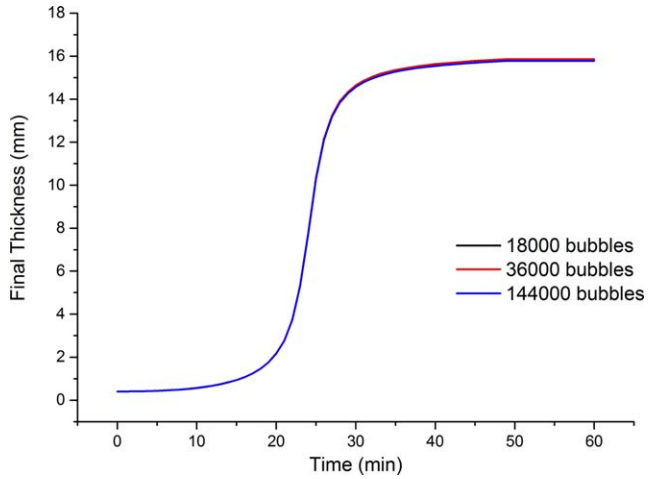


FIG. 12. Expansion-time relationship for various number of bubbles (nucleation sites). [Color figure can be viewed in the online issue, which is available at wileyonlinelibrary.com.]

explained in Section "*A Brief Introduction to the Amon and Denson Theory*." In theory, it is necessary to know the number of bubbles (nucleation sites) from which expansion occurs. However, since the nucleation sites share the same amount of gas conversion, it is expected that the expansion result would not be sensitive to the number of nucleation sites provided there is a sufficient number to smooth out the expansion. To check this, different numbers of nucleation sites have been considered in the theoretical model to investigate their influence on the final expansion thickness. Figure 11 shows the results. It can be seen that the final thickness of the intumescent coating after full expansion is the same regardless of the number of bubbles once the number of nucleation sites reached about 3600. For further investigation of this article, the total number of bubbles of 36,000 will be used, which for a 100 mm × 100 mm plate represents 60 nucleation sites in the planar direction and 10 nucleation sites in the thickness direction.

Three representative expansion-time relationships for, respectively, 18,000, 36,000, and 144,000 bubbles can be shown in Fig. 12. It can be seen that the time history of expansion is also independent of the total number of nucleation (initial bubble) sites.

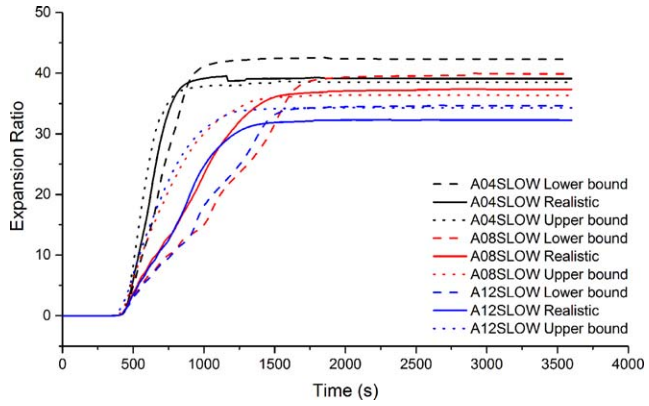


FIG. 13. Sensitivity of predicted expansion process to assumed temperature distributions, for slow fire, 5 mm steel plate thickness. [Color figure can be viewed in the online issue, which is available at wileyonlinelibrary.com.]

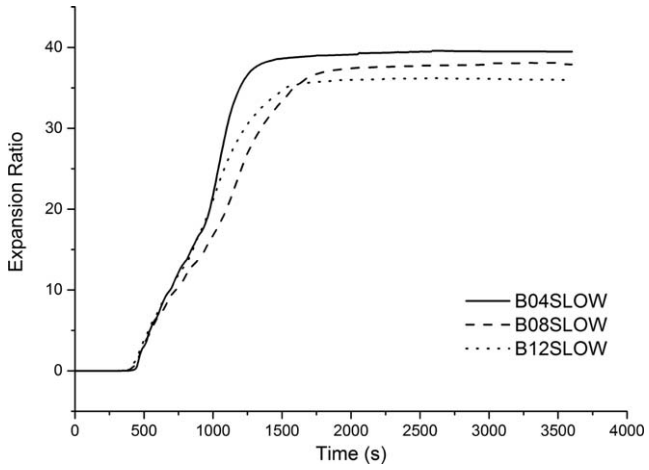


FIG. 14. Predicted expansion ratios for slow fire, 10 mm steel thickness.

*Slow Fire Results*

Figures 13–15 compare the modelling results for different coating thicknesses and different assumed temperature distributions, for 5 mm, 10 mm, and 20 mm steel plate thicknesses, respectively. Figure 13 shows that using different temperature distributions has some effect on intumescent coating expansion, but the results are quite close to each other. Therefore, for further comparisons, only the realistic temperature distribution shown in Fig. 10 will be used.

Figures 13 and 14 indicate moderate differences in the final expansion ratio under different conditions (coating thickness/steel plate thickness) for the 5 mm and 10 mm thick steel plates. However, for the 20mm thick plate tests, as shown in Fig. 15, the theoretical model predicts quite large difference in the final expansion ratios. This may be used as convincing data to support validation of the prediction results because the large reductions in expansion for C8 and C12 specimens are in excellent agreement with the test results. In fact, Table 1 compares the theoretically calculated and measured fire expansion ratios for all the slow fire tests. Despite the various assumptions of the Amon and Denson theoretical model and the further assumptions made by the authors to adapt the Amon and Denson

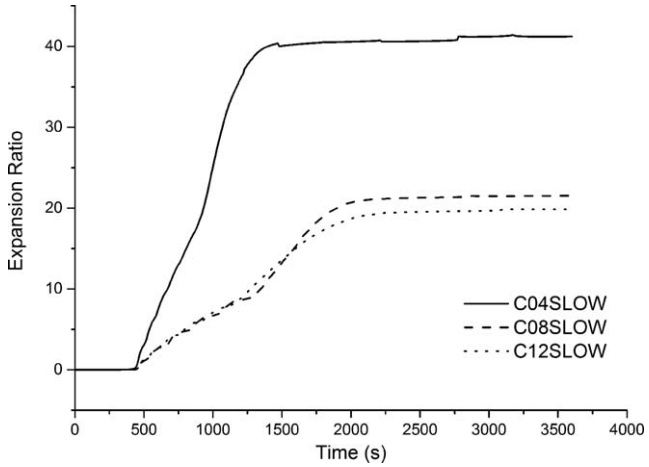


FIG. 15. Predicted expansion ratios for slow fire, 20 mm steel thickness.

TABLE 1. Comparison between measured and predicted final expansion ratios of Zhang et al. [9] with the current predictions, slow fire tests.

| Sample ID | E.R[a] measured Zhang et al. [9] | E.R[a] predicted Zhang et al. [9] | E.R[a] current prediction |
|---|---|---|---|
| A04SLOW | 39.2 | 40.8 | 39.09 |
| A08SLOW | 40.5 | 30.1 | 37.33 |
| A12SLOW | 48.6 | 31.4 | 32.27 |
| B04SLOW | 42.9 | 37.7 | 39.48 |
| B08SLOW | 39.3 | 30.5 | 37.89 |
| B12SLOW | 37.5 | 32.6 | 35.99 |
| C04SLOW | 42.3 | 28.3 | 41.22 |
| C08SLOW | 20.2 | 24.2 | 21.53 |
| C12SLOW | 16.4 | 26.4 | 19.85 |

[a] E.R, Expansion Ratio.

model, the agreement is surprisingly good. In fact, the agreement is better than that between the test results and the predictions by Zhang et al. [9].

*ISO Fire Results*

Figures 16–18 present expansion-time relationships for the ISO fire tests. Table 2 compares the theoretical expansion ratios with those measured and calculated by Zhang et al. [9]. Again, the agreement between the theoretical and measured results is quite good. It is particularly interesting to note the trend of expansion for the C-series tests whose steel plate thickness was the highest, being 20 mm. The theoretical model predicted the highest expansion ratio for the 0.8 mm DFT of A–B series tests and smallest expansion ratio C-series test compared to those of the 0.4 mm and 1.2 mm DFT tests. This is in agreement with the test observation. In contrast, the predictions of Zhang et al. [9] indicate a monotonic change in the expansion ratio as the DFT changes.

*Fast Fire Results*

Figures 19–21 compare the modelling expansion ratio results for the fast fire tests and Table 3 summarizes the final expansion results. The current theoretical results are generally in good agreement with the measured results. As can be seen from Table 3, there is a monotonic change in expansion-time relationships for each series of the fast fire test specimens. The theoretical results follow this trend except for the sample with 5 mm steel thickness (A12).

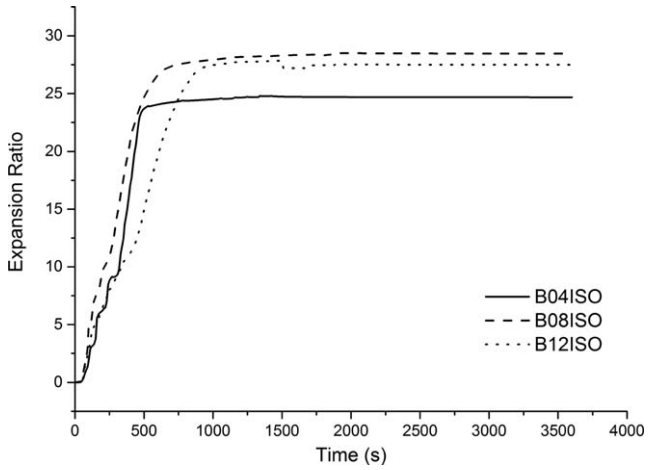


FIG. 17. Predicted expansion ratios for ISO fire tests, 10 mm steel thickness.

*Modelling the Cone Calorimeter Tests*

Figure 22 shows the cone calorimeter test set up used by Zhang et al. [10]. The same type of intumescent coating as in their furnace fire tests (Zhang et al. [9]) was used in the cone calorimeter tests. Also the same steel plate thicknesses and nominal DFTs were used. The cone calorimeter tests were performed for two levels of radiating heat flux: 50 kW/m$^2$ and 65 kW/m$^2$. The steel temperature was measured. However, there was no measurement of the intumescent coating surface temperature. In order to obtain the intumescent surface temperature to approximate the temperature profiles within the intumescent coating, the intumescent coating surface temperature $(T_{surface})$ lculation method developed by Omrane et al. [16] was used. A summary of this method is provided below:

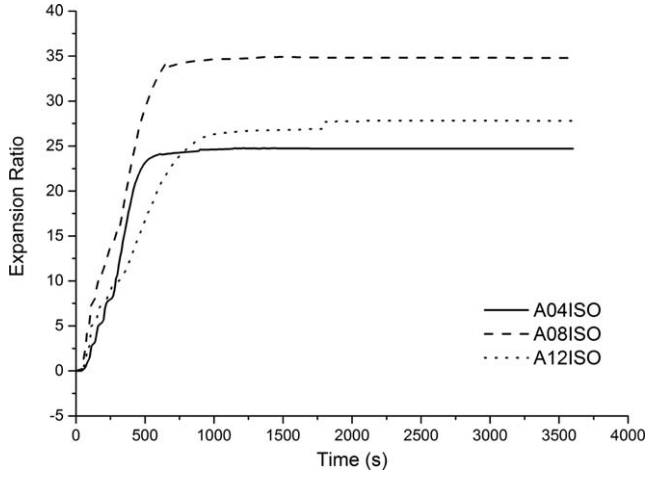


FIG. 16. Predicted expansion ratios for ISO fire tests, 5 mm steel thickness.

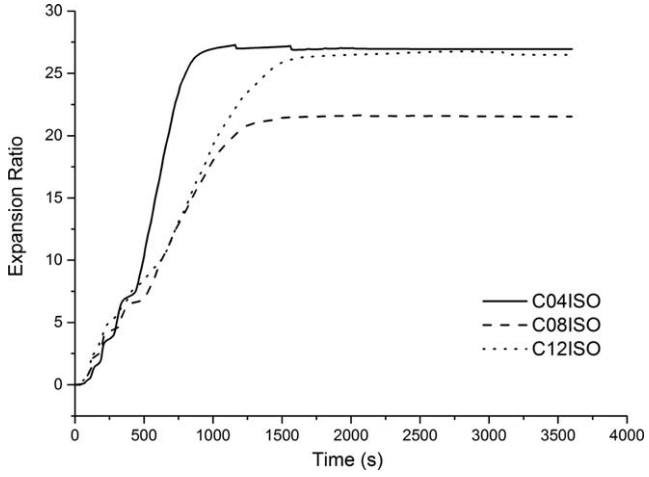


FIG. 18. Predicted expansion ratios for ISO fire tests, 20 mm steel thickness.


DOI 10.1002/pen

TABLE 2. Comparison between measured and predicted final expansion ratios of Zhang et al. [9] with the current predictions, ISO fire tests.

| Sample ID | E.R[a] measured Zhang et al. [9] | E.R[a] predicted Zhang et al. [9] | E.R[a] current prediction |
|---|---|---|---|
| A04ISO | 34.2 | 37.1 | 24.71 |
| A08ISO | 36.6 | 35.3 | 34.80 |
| A12ISO | 28.2 | 30.3 | 27.82 |
| B04ISO | 29.9 | 33.1 | 24.68 |
| B08ISO | 23.0 | 25.7 | 28.47 |
| B12ISO | 21.0 | 25.7 | 27.50 |
| C04ISO | 26.2 | 29.6 | 26.94 |
| C08ISO | 18.5 | 23.3 | 21.53 |
| C12ISO1 | 21.3 | 20.9 | 26.49 |

[a] E.R, Expansion Ratio.

Considering the test sample as one-dimensional, the surface temperature of the intumescent coating is calculated using the following heat balance equation:

$$\varepsilon\sigma T^4 + h_c(T - T_\infty) = \varepsilon Q_e - Q_{loss} - \frac{(\Delta T + \Delta T_s)}{2\Delta t}\rho_p C_p d_p - \frac{\Delta T_s}{\Delta t}\rho_s C_s d_s \quad (9)$$

where $Q_e$ is the incident irradiance (heat flux) from the cone calorimeter on the surface of the specimen, $\varepsilon$ is the surface emissivity of the intumescent coating, $h_c$ the convective heat transfer coefficient and $\rho_p, C_p, d_p$, $\rho_s, C_s, d_s$ are the density, specific heat and the original thickness of the coating and steel plate, respectively.

The first and second terms on the left-hand side of *Eq. 9* are radiation and convection heat losses from the surface of the intumescent coating to the space respectively. The first term on the right-hand side of the equation is the heat flux irradiance, the second term is the conductive heat loss from the steel plate to the mineral wool, the third and fourth terms on the right-hand side are the heat stored in the intumescent coatings and in the steel plate, respectively. In the calculation of the intumescent coating surface temperature in this study, the conductive heat loss from the steel plate to the insulation and heat stored in the coating are neglected due to good insulation and negligible coating mass, respectively. The predicted surface temperature using *Eq. 9* rapidly increases to the final steady value within 8–10 minutes.

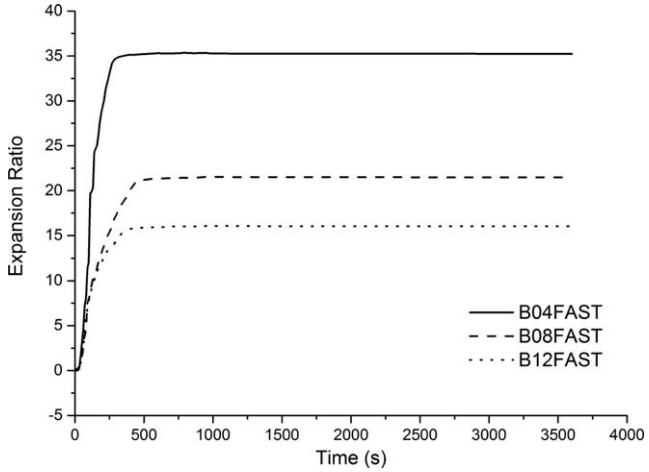


FIG. 20. Predicted expansion ratios for fast fire tests, 10 mm steel thickness.

After obtaining the intumescent coating surface temperature, the same temperature distribution profile, as shown by the middle (realistic) curve of Fig. 10, was used in the theoretical calculations using the modified Amon and Denson model.

During the cone calorimeter tests, continuous measurement of the expanded thickness of the intumescent coating was made. This makes it possible to compare the theoretical prediction of the expansion process with the test results.

In the following sections, H and L refer to heat fluxes of 65 kW/m$^2$ and 50 kW/m$^2$, respectively, whereas 1 and 2 refer to the sample number. For example, A04L1 refers to sample 1 of a 5 mm thick steel plate with 0.4 mm DFT subjected to radiant heat flux of 50 kW/m$^2$.

### *Modification to Surface Temperature Prediction*

Because some of the heat loss terms (heat conduction to insulation, heat stored in intumescent coating) in *Eq. 9* were neglected and a high surface emissivity was assumed from the

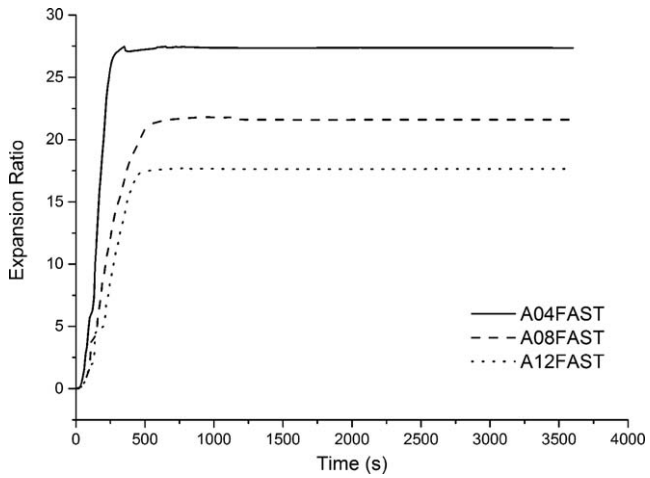


FIG. 19. Predicted expansion ratios for fast fire tests, 5 mm steel thickness sample.

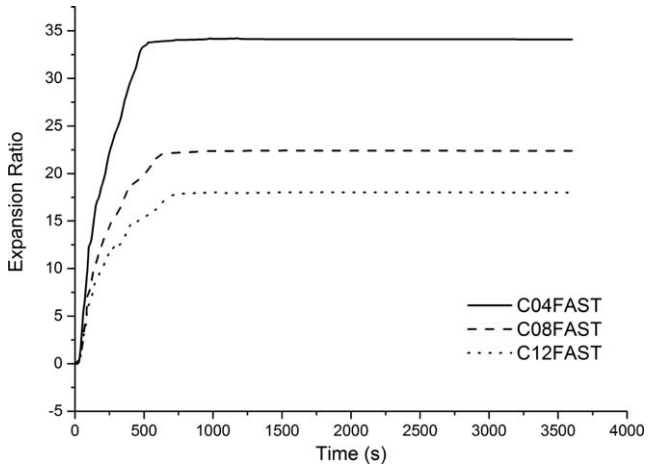


FIG. 21. Predicted expansion ratios for fast fire tests, 20 mm steel thickness.

TABLE 3. Comparison between measured and predicted final expansion ratios of Zhang et al. [9] with the current predictions, fast fire tests.

| Sample ID | E.R[a] measured Zhang et al. [9] | E.R[a] predicted Zhang et al. [9] | E.R[a] current prediction |
|---|---|---|---|
| A04FAST | 24.8 | 30.8 | 24.82 |
| A08FAST | 21.8 | 25.5 | 21.45 |
| A12FAST | 28.8 | 25.2 | 16.81 |
| B04FAST | 31.5 | 31.5 | 35.24 |
| B08FAST | 23.7 | 25.8 | 21.49 |
| B12FAST | 20.7 | 26.1 | 16.02 |
| C04FAST | 32.2 | 27.6 | 34.09 |
| C08FAST | 19.7 | 23.4 | 22.39 |
| C12FAST | 20.5 | 22.6 | 18.00 |

[a] E.R, Expansion Ratio.

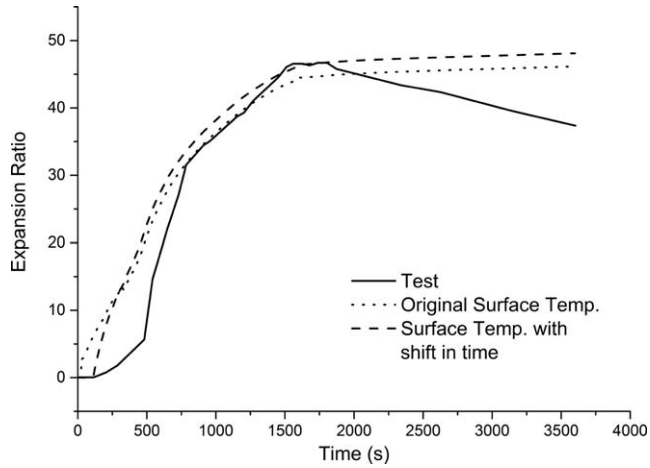


FIG. 23. Comparison of predicted and measured expansion ratios using two predicted surface temperature-time relationships (one using *Eq. 9*, one using *Eq. 9* with a shift in time), test sample B08L1.

beginning, using *Eq. 9* of Omrane et al. [16] produced very high intumescent coating surface temperature increases almost instantly from at the start of heating, causing the predicted intumescent coating expansion to increase rapidly when the experimental results indicate near zero expansion. To avoid this problem, the predicted surface temperature–time curve using *Eq. 9* were shifted by a small amount of time so that the prediction and measurement of intumescent coating thickness would start at the same time. This is shown in Fig. 23 as an example.

*Results for Low Heat Tests (50 kW/m2)*

The measured results of Zhang et al. [10] show that specimens A04L1, B08L1, and C12L1 achieved the maximum expansion, the minimum expansion and medium expansion. These three tests are used here to show detailed comparison between the theoretical prediction and test results.

Figure 24 compares the expansion ratio–time relationships for these three tests, where "Test" refers to the measured expansion ratio by Zhang et al. [10] and "Prediction" refers to the current predicted expansion ratio.

Close agreement is clearly shown between the prediction and test results for the intumescent coating expansion process and the maximum expansion ratio. The small difference may be due to the assumed coating temperature profile and it is considered acceptable. Some of the test results indicate reduction in expansion after reaching the maximum. Zhang et al. [10] attributed this to oxidation of the surface layers at high temperatures after reaching the maximum value and proposed a simplified equation, which relates the amount of mass loss after reaching full expansion to the reduction in coating thickness, to deal with this. The same procedure could have been implemented in the proposed model of this paper. However, this was considered not necessary because the main interest of this article is the

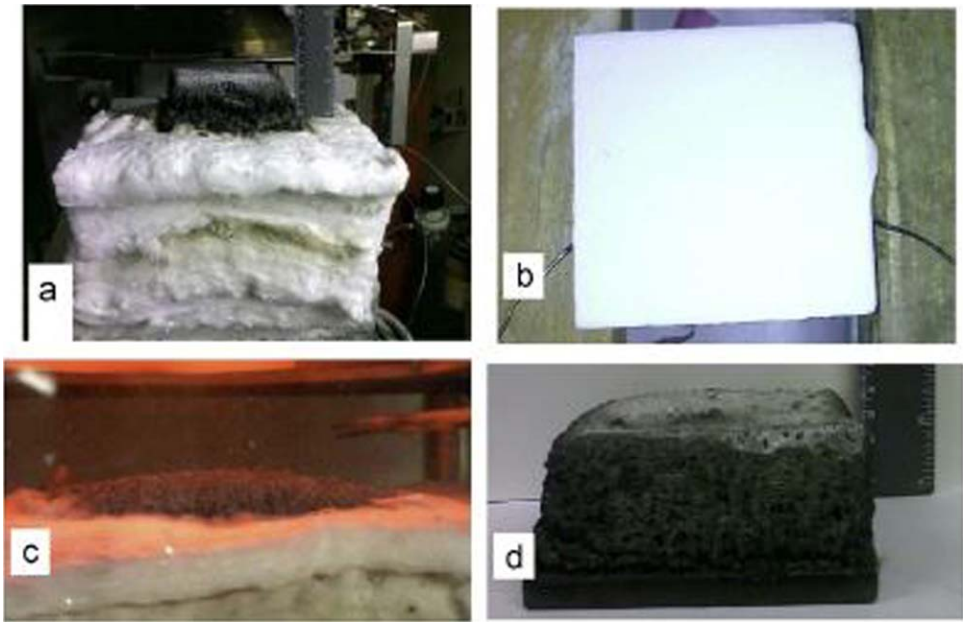


FIG. 22. (a) Experimental setup for the cone calorimeter test, (b) samples before test, (c) during test, and (d) after test. [Color figure can be viewed in the online issue, which is available at wileyonlinelibrary.com.]

 DOI 10.1002/pen

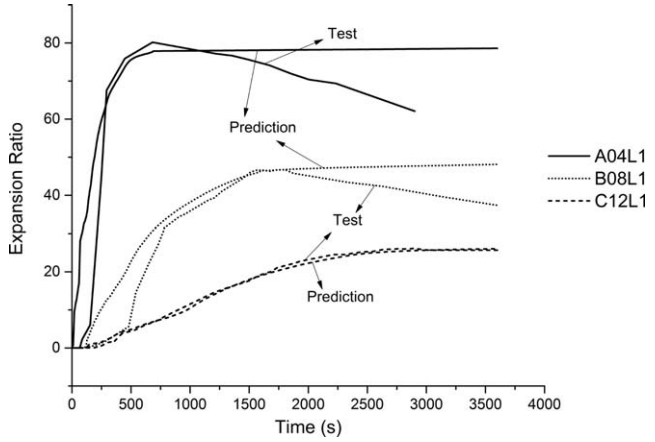


FIG. 24. Comparison of predicted and measured expansion histories for three representative tests (maximum expansion (A04), minimum expansion (C12), average expansion (B08)).

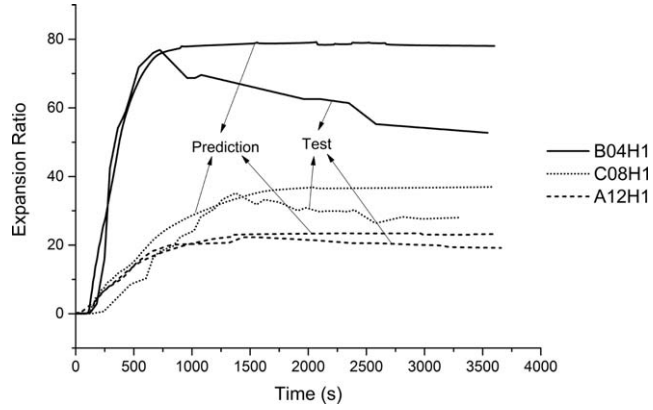


FIG. 25. Comparison between predicted and measured expansion histories for three representative (maximum expansion B04H1, minimum expansion A12H1, average expansion C08H1) of the high heat tests.

intumescent coating expansion process until reaching the maximum expansion.

Table 4 compares the predicted and measured expansion thicknesses and ratios for all the cone calorimeter tests at 50 kW/m$^2$. The predicted results from this study are the final thickness of the coatings at the end of the one hour prediction. Overall, the agreement with the measured results is very good, considering the complex physical and chemical behaviour of the intumescence process and many of the necessary assumptions may not be exact.

*Results for High Heat Tests (65 kW/m2)*

The same exercise as described above was repeated for the tests under heat flux level of 65 kW/m$^2$. Figure 25 compares the expansion ratio–time relationships for these three tests, where "Test" refers to the measured expansion ratio by Zhang et al. [10] and "Prediction" refers to the current predicted expansion ratio. Again the predicted results are again in good agreement with the measured results.

Table 5 compares the predicted and measured expansion ratios. There are some relatively large differences for some of the tests (A08H1, B04H1). This is because the measured values were the final values and the predicted values were the maximum values, and for these tests, there was a substantial amount of shrinkage after the intumescent coating had reached the maximum expansion, as shown in Fig. 25.

*Comparison Against Cone Calorimeter Tests*

Muller [12] carried out cone calorimeter tests for three different intumescent coating formulations. The steel thickness was 3 mm and the nominal DFT was 1.7 mm. The nominal heating flux was 50 kW/m$^2$, however the actual heating flux was uncontrolled and varied significantly with time. Muller [12] in fact recorded the top surface temperatures of the coatings. In the authors' prediction model, the coating surface temperatures were predicted using *Eq. 9* and the measured heat flux. The good agreement shown in Fig. 26 between the predicted surface temperatures and the recorded surface temperatures confirms that it is suitable to use the predicted surface temperatures in the proposed model.

Following the same procedure as used in Section "*Modelling the Cone Calorimeter Tests*" for the tests of Zhang et al. [10] and using the properties in Figs. 3 and 8 for the intumescent formulations of Muller [12], the proposed model was used to calculate the expansion-time relationships. Figure 27 compares the predicted and measured results. This comparison shows that the final expansions of the different intumescent coating

TABLE 4. Summary of comparison between predicted and measured thicknesses/expansion ratios of Zhang et al. [10] with the current predictions exposed to 50 kW/m$^2$.

| Sample ID | Measured final thickness (mm)/ Expansion ratio zhang et al. [10] | Predicted final thickness (mm)/ Expansion ratio Zhang et al. [10] | Current prediction final thickness (mm)/ Expansion ratio |
|---|---|---|---|
| A04L1 | 22/63 | 17.3/48.6 | 23.8/68.0 |
| A08L2 | 36/36 | 34/34.1 | 39.3/38.3 |
| A12L1 | 48/38 | 32.9/26.4 | 42.8/33.3 |
| B04L1 | 25/50 | 21.6/42 | 28.4/55.8 |
| B08L1 | 38/47 | 29.8/35.3 | 41.4/48.7 |
| B12L2 | 41/37 | 30.3/27.3 | 49.8/40.5 |
| C04L1 | 20/37 | 21.8/40.7 | 20.9/37.8 |
| C08L2 | 38/38 | 33.5/33 | 34.0/33.0 |
| C12L1 | 40/27 | 35.0/23.3 | 40.0/26.7 |

TABLE 5. Summary of comparison between predicted and measured thicknesses/expansion ratios of Zhang et al. [10] with the current predictions exposed to 65 kW/m$^2$.

| Sample ID | Measured final thickness (mm)/ Expansion ratio Zhang et al. [10] | Predicted final thickness (mm)/ Expansion ratio Zhang et al. [10] | Current prediction final thickness (mm)/ Expansion ratio |
|---|---|---|---|
| A04H1 | 21/44 | 20.5/43 | 21.3/43.5 |
| A08H1 | 26/39 | 25.6/38 | 38.2/53.6 |
| A12H1 | 31/19 | 37.4/23 | 37.5/23.4 |
| B04H1 | 13/46 | 13.5/48 | 21.2/75.7 |
| B08H1 | 26/39 | 25.6/38 | 31.7/44.2 |
| B12H1 | 38/25 | 37.6/25 | 45.4/29.2 |
| C04H1 | 21/37 | 19.8/35 | 24.8/44.1 |
| C08H1 | 24/30 | 29.7/37 | 31.7/38.2 |
| C12H1 | 35/28 | 32.3/26 | 37.8/29.5 |

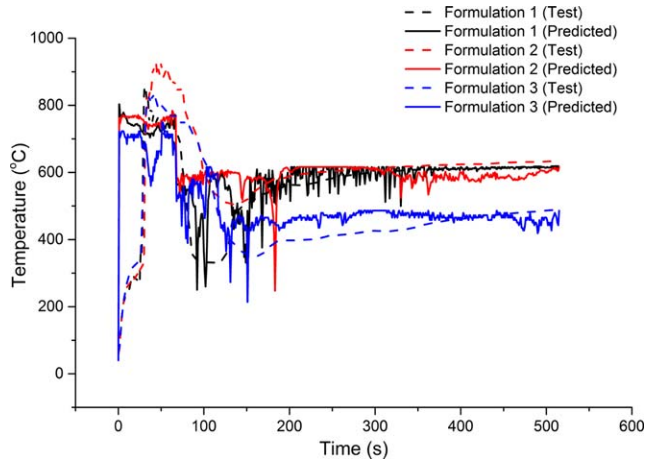


FIG. 26. Comparison of surface temperatures for Muller [12] tests. [Color figure can be viewed in the online issue, which is available at wileyonlinelibrary.com.]

formulations and the times to reach them have been predicted with a good degree of accuracy. However, there are relatively large discrepancies before reaching the maximum expansion. This was likely caused by bubble bursting at the surface at the very early stage of heating, and this phenomenon cannot be predicted using the current modified Amon and Denson mathematical model. However, because the surface layer is very thin, and the protected steel temperature, which is the ultimate interest in predicting intumescent coating behaviour, is only moderately affected by the initial intumescent coating expansion, no refinement of the prediction model has been attempted. For confirmation, Fig. 28 compares the predicted temperatures for the protected steel plates for the three tests using the predicted expansion-time relationships and using the measured expansion-time relationships, and with the measured steel plate temperatures. The very large differences in the expansion-time relationships at the early stage of heating have only small effects on the maximum steel temperatures.

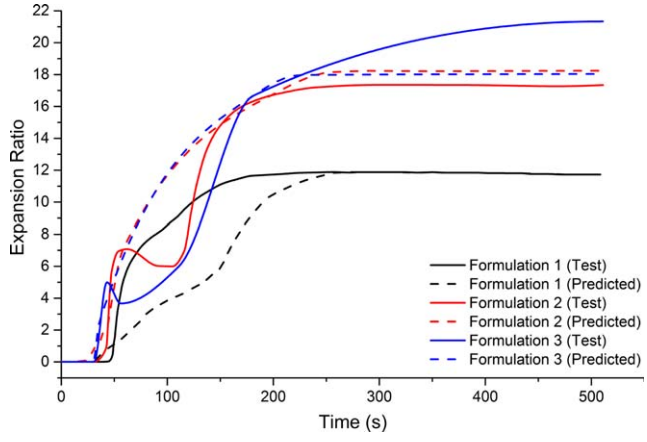


FIG. 27. Comparison of the expansion ratios between the recorded data by Muller [12] and the proposed prediction model. [Color figure can be viewed in the online issue, which is available at wileyonlinelibrary.com.]

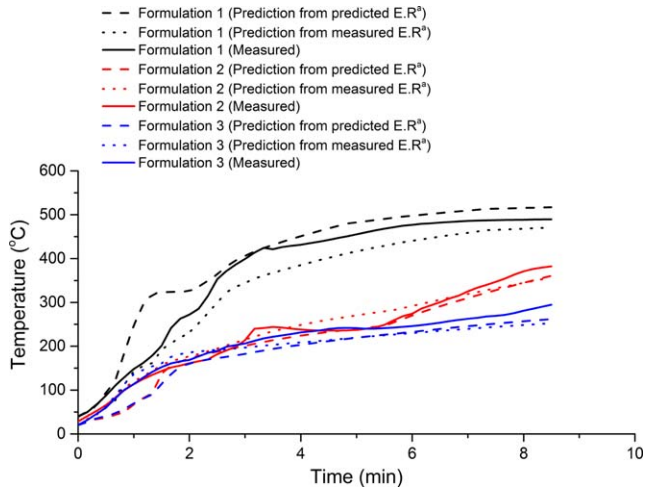


FIG. 28. Comparison of predicted steel temperatures using the predicted and measured expansion–time relationships and with the measured steel temperatures ([a]E.R: Expansion Ratio). [Color figure can be viewed in the online issue, which is available at wileyonlinelibrary.com.]

## CONCLUSIONS

This article has assessed the feasibility of extending the theoretical model of Amon and Denson [11] to predict expansion of intumescent coating in fire. The Amon and Denson theoretical model calculates the rate of increase in diameter of spherical bubbles in viscous liquid when the pressure inside bubbles increases. For application to the calculation of intumescent coating expansion, the driving pressure comes from conversion of intumescent melt to gases. The main extensions to the Amon and Denson model include non-uniform temperature field and temperature-dependent viscosity. Calculation results from the extended Amon and Denson [11] model have been compared to the cone calorimeter test results of Zhang et al. [10] the furnace fire test results of Zhang et al. [9], and the cone calorimeter tests of Muller [12]. These tests included different intumescent coating formulations, different steel plate thicknesses, different intumescent coating thicknesses and different fire/cone calorimeter heating conditions. The following conclusions may be drawn:

The extended model prediction results are insensitive to the number of initial nucleation sites (where the expanding bubbles start) provided a sufficiently large number is used. The surface temperature of the intumescent coating melt has minor effect on expansion.

Expansion of the same intumescent coating varies depending on the heating condition. This variation is not monotonic with heating rate. The extended Amon and Denson model has been demonstrated to give prediction results of the maximum intumescent coating expansion in good agreement with the measured results of Zhang et al. [9, 10] and Muller [12].

Bubble bursting at the thin surface layer may introduce some inaccuracy in predicting the expansion process during the initial heating phase before reaching full expansion of the intumescent coatings, however, the effect on the maximum expansion is very small. Furthermore, the predicted temperatures for the protected steel plates are not very sensitive to these differences.

## REFERENCES

1. CEN, "EN 13381-8:2013 Test Methods for Determining the Contribution to the Fire Resistance of Structural Members", in

 DOI 10.1002/pen

*Part 8. Applied Passive Protection Products to Steel Member*, BSI: London (2013).
2. D.E. Cagliostro, S.R. Riccitello, K.J. Clark, and A.B. Shimizu, *J. Fire Flamm.*, **6**, 205 (1975).
3. J.D.J. Anderson, E. Charles, and D.K. Wauters, *Int. J. Eng. Sci.*, **22**, 881 (1984).
4. J.B. Henderson and T.E. Wiecek, *J. Comp. Mater.*, **21**, 373 (1987).
5. C. Di Blasi and C. Branca, *AIChE J.*, **47**, 2359 (2001).
6. C. Di Blasi, *J. Anal. Appl. Pyrolysis*, **71**, 721 (2004).
7. J.F. Yuan, and Y.C. Wang, "Chapter 15 Efficient Modelling of Temperatures in Steel Plates Protected by Intumescent Coating in Fire," in *Fire Retardancy of Polymers: New Strategies and Mechanisms*, The Royal Society of Chemistry, (2009).
8. K.M. Butler, H.R. Baum, and T. Kashiwagi, "Three-dimensional Modeling of Intumescent Behaviour in Fires," in *Proceedings of the Fifth International Symposium*, Melbourne, Australia: International Association for Fire Safety Science (1997).
9. Y. Zhang, Y.C. Wang, C.G. Bailey, and A.P. Taylor, *J. Fire Sci.*, **31**, 51 (2012).
10. Y. Zhang, Y.C. Wang, C.G. Bailey, and A.P. Taylor, *Fire Safety J.*, **50**, 51 (2012).
11. M. Amon and C.D. Denson, *Polym. Eng. Sci.*, **24**, 1026 (1984).
12. M. Muller, "Systemic Approach of the Synergism in Flame Retarded Intumescent Polyurethanes," Doctor of Philosophy Université Lille 1 (2012).
13. D.Y. Kwok, L.K. Cheung, C.B. Park, and A.W. Neumann, *Polym. Eng. Sci.*, **38**, 757 (1998).
14. M. Bugajny, M.L. Bras, and S. Bourbigot, *Fire Mater.*, **23**, 49 (1999).
15. S. Bourbigot, M.L. Bras, S. Duquesne, and M. Rochery, *Macromol. Mater. Eng.*, **289**, 499 (2004).
16. A. Omrane, Y.C. Wang, U. Göransson, G. Holmstedt, and M. Aldén, *Fire Safety J.*, **42**, 68 (2007).